

# Power Allocation in Cognitive Satellite-Vehicular Networks From Energy-Spectral Efficiency Tradeoff Perspective

Yuhan Ruan<sup>1</sup>, Member, IEEE, Yongzhao Li<sup>2</sup>, Senior Member, IEEE, Cheng-Xiang Wang<sup>3</sup>, Fellow, IEEE, Rui Zhang, and Hailin Zhang<sup>4</sup>, Member, IEEE

**Abstract**—With great potential to support multitudinous services and applications in intelligent transportation systems, cognitive satellite-vehicular networks, an emerging paradigm of cognitive satellite-terrestrial networks, are attracting increasing attentions. To realize friendly coexistence of satellite and vehicular networks as well as efficient resource utilization, we investigate power allocation for the cognitive satellite-vehicular network under a realistic 3-D vehicle-to-vehicle channel model. Specifically, by analyzing the characteristics of energy efficiency (EE) and spectral efficiency (SE) performance in different vehicular environments, we first develop an EE–SE tradeoff metric with a preference factor. Based on the developed metric, we formulate and analyze a power allocation strategy from the EE–SE tradeoff perspective while guaranteeing the interference power constraint imposed by satellite communications. Further, utilizing the obtained optimal transmit power, we derive a closed-form expression of the outage probability, through which the impacts of the preference parameter and interference constraints on the performance of vehicular communications can be theoretically analyzed. Finally, numerical results are provided to demonstrate the viability of the EE–SE tradeoff metric and the validity of theoretical analyses.

**Index Terms**—Cognitive satellite-vehicular networks, power allocation, energy-spectral efficiency, interference constraints, outage probability.

## I. INTRODUCTION

**B**ENEFITING from the advantages of both satellite and terrestrial systems, hybrid satellite-terrestrial networks are becoming a promising infrastructure to enhance spectral

efficiency (SE), extend system coverage, and increase service availability and resilience [1], [2]. However, with the increasingly growing number of applications and services in satellite communications as well as fifth-generation (5G) communications, the available frequency resources have become scarce due to the dedicated frequency allocation of standardized wireless systems [3], [4]. Recently, cognitive radio (CR) which makes use of spectrum more intelligently and flexibly has widely been regarded as an effective means to alleviate the spectrum shortage. In this context, the incorporation of CR techniques into satellite-terrestrial networks, referred to as cognitive satellite-terrestrial networks, have attracted tremendous attention in academic research [5], [6], standardization, e.g., European Telecommunications Standards Institute (ETSI) [7], and applications, e.g., tactical data links [8].

Until now, numerous researchers have devoted to the spectrum sharing between satellite and terrestrial networks. Maleki *et al.* [9] presented several basic scenarios and system models for cognitive satellite-terrestrial networks, where satellite and terrestrial networks can operate as primary and secondary systems, respectively, or vice versa. In regard to spectrum sharing, cognitive satellite-terrestrial networks can operate on various modes, e.g., underlay, overlay, and interweave [10], [11]. The underlay mode, in which the cognitive system is allowed to share the spectrum licensed to the primary user, is especially attractive due to its effective spectrum utilization. In this context, various resource allocation schemes were studied to optimize the performance of cognitive satellite-terrestrial networks [12]–[17]. Specifically, Lagunas *et al.* [12] proposed a carrier-power-bandwidth allocation scheme to maximize the satellite throughput. Vassaki *et al.* [13] introduced a power allocation scheme that can optimize the effective capacity of terrestrial communications for given quality of service (QoS) requirements while guaranteeing the outage probability (OP) of satellite communications. Li *et al.* [14] conducted power allocation to maximize the achievable rate for cognitive hybrid satellite-terrestrial networks with amplify-and-forward (AF) relays. For real-time satellite applications in cognitive satellite-terrestrial networks, Shi *et al.* [15] conducted power control to maximize the delay-limited capacity without degrading the communication quality of the primary terrestrial user. Besides, to enhance the physical layer security for cognitive satellite terrestrial networks,

Manuscript received October 18, 2018; revised February 9, 2019; accepted March 9, 2019. Date of publication March 14, 2019; date of current version June 7, 2019. The authors acknowledge the support from the National Key R&D Program of China under Grant 2016YFB1200202, the National Natural Science Foundation of China under Grant 61771365, the Natural Science Foundation of Shaanxi Province under Grant 2017JZ022, the Postdoctoral Science Foundation of China under Grant 30101180044, the 111 Project under Grant B08038, the Fundamental Research Funds for the Central Universities under Grant 2242019R30001, and the EU H2020 RISE TESTBED project under Grant 734325. The associate editor coordinating the review of this paper and approving it for publication was A. Zanella. (*Corresponding author: Rui Zhang.*)

Y. Ruan, Y. Li, R. Zhang, and H. Zhang are with the State Key Laboratory of Integrated Services Networks, Xidian University, Xi'an 710071, China (e-mail: ryh911228@163.com; yzhli@xidian.edu.cn; rui.zhang@stu.xidian.edu.cn; hlzhang@xidian.edu.cn).

C.-X. Wang is with the National Mobile Communications Research Laboratory, School of Information Science and Engineering, Southeast University, Nanjing 210096, China, and also with the Purple Mountain Laboratories, Nanjing 211111, China (e-mail: chxwang@seu.edu.cn).

Digital Object Identifier 10.1109/TCCN.2019.2905199

beamforming based secure transmissions were studied in [16] and [17].

On the other hand, with the development of industry and economy, vehicular communications have been encountered in many applications, such as wireless mobile ad-hoc peer-to-peer networks and intelligent transportation systems. To keep pace with 5G communications and support satellite communications in mobile environments, e.g., emergency relief vehicles, satellite-vehicular communication is becoming a popular research topic. Through simulations, Nguyen *et al.* [18] evaluated the practical achievable capacity of satellite vehicular communications operating in X, Ku, and Ka bands. Cocco *et al.* [19] employed network coding to combat severe channel fading and extend the satellite coverage in land mobile satellite vehicular networks. These studies demonstrated the feasibility and prospect of realizing vehicular communications in satellite-terrestrial networks.

Inspired by the benefits of applying CR to satellite-terrestrial networks and the development of vehicular communications, in this paper, we focus on a cognitive satellite-vehicular network, which is a visualized and concrete application of cognitive satellite-terrestrial networks in mobile environments. Specifically, the satellite network is regarded as the primary system and the vehicular network operates as the secondary system. To realize the coexistence of satellite and vehicular networks in the underlay mode, efficient resource allocation is a significant challenge in vehicular environments.

Although resource allocation schemes in cognitive satellite-terrestrial networks have been extensively investigated, these studies mainly analyzed and optimized the performance of satellite-terrestrial networks from the perspective of SE. Energy efficiency (EE) is also a vital performance metric in the design of future environment-friendly satellite communications [20]–[22]. Thus, consideration of both SE and EE is of great importance for green cognitive satellite-terrestrial communication networks. Unfortunately, it is well known that EE and SE efficient transmission techniques are inconsistent with each other and there exists a tradeoff between EE and SE [23]. Zhang *et al.* [24] investigated the EE-SE tradeoff by optimizing EE with the SE constraint in hybrid satellite-terrestrial networks. However, in the cognitive satellite-vehicular network, the mobility of vehicular users and the vehicular traffic density (VTD) can greatly affect the signal propagation and subsequently pose new challenges in radio resource management [25]. Therefore, the tradeoff formulations as in [24], optimizing either SE or EE, is not suitable for vehicular communications with different applications and dynamic surrounding circumstances.

Motivated by this need, in this paper, we investigate power allocation from a novel EE-SE tradeoff perspective in cognitive satellite-vehicular networks, where the vehicular link is modeled as a three-dimensional (3D) vehicle-to-vehicle (V2V) channel to characterize the mobility of vehicular users and the VTD in a realistic vehicular environment [26]. By analyzing the characteristics of EE-SE performance in different VTD scenarios, we firstly develop a unified EE-SE tradeoff metric. To efficiently manage the co-channel interference caused by

spectrum reuse, we derive and analyze a power allocation strategy based on the developed EE and SE tradeoff metric. The major contributions of this paper are summarized as follows:

- 1) A unified EE and SE tradeoff metric is proposed for power allocation in cognitive satellite-vehicular networks. According to the observations of EE-SE performance in different VTD scenarios, it makes much sense to optimize SE in a high VTD scenario while pursue EE in a low VTD scenario for power allocation in cognitive satellite-vehicular networks. To make the optimization more tractable than conventional individual optimizations, we condense the SE and EE into a single utility function with a preference factor. Through this preference factor, the priority level of EE and SE can be flexibly adjusted to adapt to dynamic surrounding circumstances. In addition, we prove the utility function is strictly quasi-convex in transmit power.
- 2) Based on the developed EE-SE tradeoff metric, the optimal power allocation is derived and analyzed. Firstly, taking the mutual interference into account, we formulate the power allocation scheme as an optimization problem that minimizes the utility function of vehicular communications while guaranteeing the interference power constraints imposed by satellite communications. Then, employing the Charnes-Cooper transformation [27], we transform the fractional optimization problem into an equivalent convex problem and derive the optimal solution of the transmit power.
- 3) Utilizing the derived optimal transmit power, we analyze the outage performance and obtain a closed-form expression of the OP in cognitive satellite-vehicular networks, where the communication link and interference links are modeled as 3D V2V channel and generalized- $K$  channels, respectively. Through the obtained closed-form expression, the impact of the preference parameter and interference constraints on the performance of vehicular communications can be theoretically analyzed.

The remainder of the paper is organized as follows. Section II introduces the system model of the cognitive satellite-vehicular network. Section III develops a unified EE and SE tradeoff metric and investigates a power allocation scheme. Based on the obtained optimal transmit power, we discuss the tradeoff between EE and SE and theoretically analyze the outage performance in Section IV. Section V numerically evaluates the developed power allocation scheme and show the effect of various parameters on the EE and SE tradeoff. Finally, conclusions are given in Section VI.

## II. SYSTEM MODEL

In this paper, we consider a cognitive satellite-vehicular network as illustrated in Fig. 1. Similar to [13], the satellite network acts as the primary system and shares downlink spectral resource with the terrestrial vehicular network, referred to as the secondary system. In this case, the secondary vehicular transmitter (ST) will interfere the primary receiver (PR) while the secondary vehicular receiver (SR) will also suffer from the interference caused by the primary transmitter (PT). It is

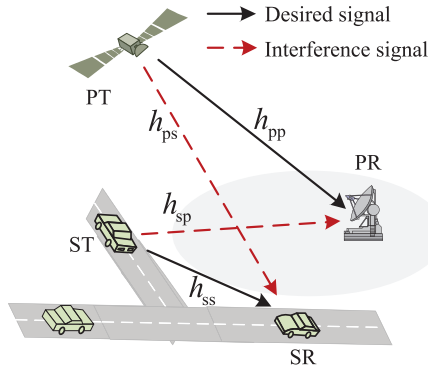


Fig. 1. An underlay cognitive satellite-vehicular network.

assumed that each node is equipped with a single antenna and operates in a half-duplex mode.<sup>1</sup> We denote  $h_{ss}$  and  $h_{pp}$  as the channel coefficients of  $ST \rightarrow SR$  and  $PT \rightarrow PR$  communication links, respectively, while  $h_{ps}$  and  $h_{sp}$  as the channel coefficients of  $PT \rightarrow SR$  and  $ST \rightarrow PR$  interfering links, respectively.<sup>2</sup>

#### A. Signal Model

For the secondary system, the signal received at the vehicular receiver can be expressed as

$$y = \sqrt{P_s}h_{ss}x + \sqrt{P_p}h_{ps}z + n \quad (1)$$

where  $P_s$  and  $P_p$  are the transmit powers of the vehicular transmitter and the satellite, respectively,  $x$  represents the desired signal from the vehicular transmitter,  $z$  denotes the interference signal from the satellite communication,<sup>3</sup>  $n$  represents the complex additive white Gaussian noise (AWGN) with power  $N_0$ .

Given a system bandwidth  $W$ , the spectral efficiency ( $\Psi_{SE}$ , in bits/s/Hz) of V2V communications can be expressed as

$$\Psi_{SE} = \frac{\mathbb{E}\{C\}}{W} = \mathbb{E}\{\log_2(1 + \gamma_s)\} \quad (2)$$

where  $\mathbb{E}\{\cdot\}$  denotes the expectation operator,  $C$  is the instantaneous capacity, and  $\gamma_s = \frac{P_s|h_{ss}|^2}{N_0 + P_p|h_{ps}|^2}$  is the received signal-to-interference-plus-noise ratio (SINR) at the vehicular receiver.

Energy efficiency ( $\Psi_{EE}$ , in bits/Joule/Hz) is defined as the ratio of  $\Psi_{SE}$  to the total power expenditure ( $P_{tot}$ , in Watt)

<sup>1</sup>Since this paper mainly focuses on managing the interference caused by frequency reuse in underlay cognitive satellite-vehicular networks and thus assumes that each node works in half-duplex mode. The self-interference elimination and other key technologies for full-duplex communications [28] are out of the scope of this paper.

<sup>2</sup>Similar to [29], we assume that these channels are quasi-static and the corresponding instantaneous channel state information can be obtained by adopting the sparsity structure based channel estimation approach proposed in [30]. How to reduce the amount of feedback to make the proposed power allocation scheme more feasible in practical implications is left for our future research.

<sup>3</sup>Although the satellite is far away from the vehicular receiver, when the vehicular receiver is located in the beam footprint of the satellite or the channel condition is good between the satellite and the vehicular receiver, the interference from the satellite cannot be ignored.

and can be formulated as

$$\Psi_{EE} = \frac{\Psi_{SE}}{\mathbb{E}\{P_{tot}\}} \quad (3)$$

where  $P_{tot}$  consists of radio-frequency power  $\eta P_s$ , circuit power  $P_0^C$ , and static power  $P_0^S$ , i.e.,  $P_{tot} = \eta P_s + P_0^C + P_0^S$ . Here,  $\eta$  is the transmit power consumption coefficient that scales up with the transmit power due to amplifier loss. Intuitively,  $\eta \in [1, \infty)$  is the reciprocal of the power amplifier efficiency which varies in the range of  $(0, 1]$  [31]. Since the circuit and static power consumptions are usually independent of data rate and can be regarded as constants for the transmitter, for notational simplicity, we use  $P_{tot} = \eta P_s + P_0$  in the following, where  $P_0 = P_0^C + P_0^S$ .

#### B. Channel Model

From Fig. 1 we can observe that the considered cognitive satellite-vehicular network involves two kinds of channel. One is the conventional fixed-to-mobile/fixed channel and the other is the V2V channel where both the transmitter and receiver are in motion. Specifically, the conventional fixed-to-mobile/fixed links consist of one terrestrial link ( $h_{sp}$ ) and two land mobile satellite (LMS) links ( $h_{pp}$  and  $h_{ps}$ ). As demonstrated, the generalized- $K$  model can properly describe not only the signal propagation on terrestrial links [32], but also the channel environment of satellite communications [21]. Considering the broad suitability of the generalized- $K$  model, we model these links uniformly as the generalized- $K$  distribution. The generalized- $K$  distribution is a mixture of Gamma-distributed shadowing and Nakagami-distributed multipath fading effect.

For the generalized- $K$  model, the PDF of  $|h_i|^2$  ( $i = pp, ps, sp$ ) can be written as

$$f_{|h_i|^2}(x) = \frac{2b_i^{\varphi_i + \varepsilon_i}}{\Gamma(\varepsilon_i)\Gamma(\varphi_i)} x^{\left(\frac{\varphi_i + \varepsilon_i}{2}\right) - 1} K_{\varphi_i - \varepsilon_i}(2b_i\sqrt{x}) \quad (4)$$

where  $K_{\varphi_i - \varepsilon_i}(\cdot)$  is the modified Bessel function of the second kind with order  $(\varphi_i - \varepsilon_i)$  and  $b_i = \sqrt{\frac{\varphi_i \varepsilon_i}{\Omega_i}}$ . Here,  $\varepsilon_i \geq 0.5$  and  $\varphi_i \geq 0$  are the multipath and shadowing parameters, respectively,  $\Omega_i$  is the mean of the received local power. Since the generalized- $K$  distribution has a relatively simple mathematical form, it allows an integrated performance analysis of digital communication systems operating in composite multipath/shadowing fading environments.

Apart from the conventional fixed-to-mobile/fixed links, the considered network also involves V2V links in the secondary vehicular communications, where both the transmitter and receiver may have high mobility. In this paper, we adopt a simple vehicle-mobility model where vehicles move in a straight line with a constant velocity. Under this situation, the traditional channel model where either the transmitter or the receiver is assumed motionless is no longer applicable. Therefore, we adopt the 3D V2V channel model proposed in [26] to accurately capture the effect of the velocity and VTD on the channel characteristics. In this model, the radio propagation environment is characterized by 3D effective scattering with line-of-sight (LoS) and non-LoS (NLoS) components between the vehicular transmitter and receiver. Specifically, the

NLoS components can be further classified as single bounced (SB) rays representing signals reflected only once during the propagation process and double bounced (DB) rays representing signals reflected more than once. Noteworthy, different from physical scatterers, an effective scatterer may include several physical scatterers which are unresolvable in delay and angle domains. Moreover, this channel model utilizes a two-sphere model to mimic the moving scatterers, such as other vehicles, and an elliptic-cylinder model to depict the stationary roadside environments, such as buildings and trees. The geometry of the single- and double-bounced two-sphere model and other related details can be found in [26].

The channel coefficient<sup>4</sup>  $h_{ss}$  at the carrier frequency  $f$  is a superposition of three types of components, which can be expressed as

$$h_{ss} = h_{LoS} + \sum_{i=1}^I h_{SB_i} + h_{DB} \quad (5)$$

where  $h_{LoS}$ ,  $h_{SB_i}$ , and  $h_{DB}$  are the LoS component, SB component, and DB component, respectively. In this model,  $I = 3$ , which means there are three subcomponents for SB rays, i.e.,  $SB_1$  from the transmitter sphere,  $SB_2$  from the receiver sphere, and  $SB_3$  from the elliptic-cylinder. According to [26], the probability density function (PDF) of  $|h_{ss}|^2$  can be expressed as

$$f_{|h_{ss}|^2}(x) = (1 + K)e^{-K} e^{-(1+K)x} I_0\left(2\sqrt{K(1+K)x}\right) \quad (6)$$

where  $K$  is the Ricean factor and  $I_0(x)$  is the zero-order modified Bessel function of the first kind.

### III. POWER ALLOCATION IN COGNITIVE SATELLITE-VEHICULAR NETWORKS FROM EE-SE TRADEOFF PERSPECTIVE

In this section, we investigate a power allocation strategy for cognitive satellite-vehicular networks. According to the distinct performance characteristics in different VTD scenarios, a unified EE-SE tradeoff metric is firstly developed to facilitate the applicability and tractability of resource management. By proving the utility function being strictly quasi-convex in transmit power, we propose an optimal power allocation scheme for vehicular communications to minimize the utility function under the interference power constraints imposed by satellite communications. Moreover, with the Charnes-Cooper transformation, the optimal solution for the transmit power is derived.

#### A. A Unified Spectral-Energy Efficiency Tradeoff Metric

To design a delicate power allocation strategy from the EE-SE tradeoff perspective, first, we need to analyze the performance characteristics of EE and SE in cognitive satellite-vehicular networks. In vehicular communications, high VTD and low VTD scenarios are two typical scenarios corresponding to communication occurs in urban and rural areas, respectively. In a high VTD scenario with dozens of vehicles per square kilometer, the received power comes from all

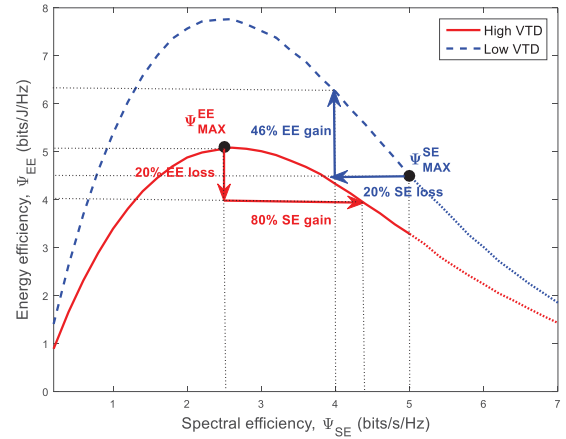


Fig. 2. EE versus SE in cognitive satellite-vehicular networks with different VTD scenarios ( $d_{ss} = 300$  m,  $v = 10$  m/s,  $P_0 = 150$  mW,  $\bar{\gamma}_p = 8$  dB,  $I_{th} = -90$  dBm).

directions reflected by moving vehicles and DB rays dominate due to dense moving vehicles. In a low VTD scenario with less than ten vehicles per square kilometer, the received power comes mainly from specific directions identified by main stationary roadside scatterers and LoS component. It is interesting to note that the Ricean factor  $K$  specified in (6) in a low VTD scenario is larger than that in a high VTD scenario, indicating that a better channel performance can be achieved in a low VTD scenario compared with the high VTD case. As illustrated in [26] and [33], the VTD has a great impact on all channel statistical properties, which eventually affect the performance of EE and SE.

In the following, to explicitly reveal the impact of VTD on EE and SE, we plot the achievable EE versus SE for V2V communications in different VTD scenarios in Fig. 2. As expected, the EE increases at the beginning and decreases afterwards in both scenarios, verifying the tradeoff between EE and SE. However, the slopes of two curves that EE versus SE are distinguishing. For example, as can be seen in Fig. 2, for the high VTD scenario, a small degradation in EE (20%) around its peak value results in a significant gain in SE (80%). While for the low VTD scenario, we can achieve a considerable gain in EE (46%) with a small degradation in SE (20%). These observations illustrate that it would make much sense to optimize SE in high VTD scenario while optimize EE in low VTD scenario.

The above observations and discussions reveal different preference of EE and SE in various vehicular scenarios. However, the existing literature mainly optimized either EE or SE with the requirement of the other one as the same when conducting power allocation, which is only suitable for specific communication scenarios and cannot deal with the dynamic changes of circumstances. Moreover, both EE and SE are considered as two key performance indicators for 5G communication systems. As such, EE and SE should jointly be maximized as a multi-objective optimization problem (MOOP). Here, we need to note two phenomena. Firstly, due to the fact that EE and SE functions are correlated and the curve of

<sup>4</sup>Time index is omitted in this paper for notation simplicity.

EE-SE relation turns to a bell shape, maximizing EE and SE are conflicting objectives and can hardly be achieved simultaneously. Secondly, from Fig. 2 we can see that for vehicular communications, VTD has impacts on the system preference of EE and SE. To facilitate the applicability and tractability of resource management, we aim to develop a power allocation scheme which is capable to adapt to diverse propagation characteristics of vehicular environments.

Inspired by the green communication trend and the diversity of preferences in different VTD scenarios, we adopt the weighted sum method to convert the MOOP into a new EE-SE tradeoff framework with a synthetic objective. Considering the unit for EE is bits/Joule/Hz while the unit for SE is bits/s/Hz, to get rid of the different measurements and orders of magnitude of EE and SE, we first normalize the EE and SE with the corresponding maximum achievable EE value, i.e.,  $\Psi_{\text{MAX}}^{\text{EE}}$ , and SE value, i.e.,  $\Psi_{\text{MAX}}^{\text{SE}}$ , respectively. Here,  $\Psi_{\text{MAX}}^{\text{EE}}$  and  $\Psi_{\text{MAX}}^{\text{SE}}$  represent the maximum values achievable on the feasible region of transmit power, i.e.,  $P \in [0, I_{\text{th}}/|h_{\text{sp}}|^2]$ . In this way, the SE and EE can be regarded as quantities without an associated physical unit. From Fig. 2 we can see that, it makes much sense to maximize  $\text{EE}(P_s) = \frac{\Psi_{\text{MAX}}^{\text{EE}}}{\Psi_{\text{MAX}}^{\text{SE}}}$  in a low VTD scenario while turns to  $\text{SE}(P_s) = \frac{\Psi_{\text{MAX}}^{\text{SE}}}{\Psi_{\text{MAX}}^{\text{EE}}}$  in a high VTD scenario. In other words, it is equivalent to minimize  $\text{EE}^{-1}(P_s)$  and  $\text{SE}^{-1}(P_s)$ , respectively. By denoting  $\omega$  and  $1 - \omega$  as the relative preference factors of EE and SE, we formulate the unified metric as

$$\mathcal{F}(\omega, P_s) = (1 - \omega) \frac{\Psi_{\text{MAX}}^{\text{SE}}}{\Psi_{\text{SE}}} + \omega \frac{\Psi_{\text{MAX}}^{\text{EE}}}{\Psi_{\text{EE}}}. \quad (7)$$

It can be seen that through the preference factor  $\omega$ , the priority level of EE and SE can be flexibly changed to adapt to different VTD scenarios, thus various vehicular environments. It is worthy noting that although different VTD scenarios have different preference of EE and SE from the perspective of enhancing system resource efficiency, we cannot obtain an optimal  $w$  value. This is because in practical applications,  $w$  is the priori articulation of preference for EE and SE provided by system operator, based on the specific situation of the system resources. To make the subsequent power allocation tractable, we give the following theorem.

*Theorem 1:* For any fixed weight  $\omega$ , the utility function  $\mathcal{F}(\omega, P_s)$  is strictly quasi-convex in  $P_s$ .

*Proof:* The proof is presented in Appendix A. ■

### B. The Optimal Power Allocation Derivation

Based on the developed utility function, a power allocation scheme is then proposed for better coexistence of the vehicular and satellite communications. In the power allocation, we minimize the utility function of vehicular communications while restricting the interference power imposed at the satellite receiver below a predefined threshold, i.e.,  $I_{\text{th}}$ . Considering the services in vehicular communications are mostly determined by instant SINR [34], we adopt the peak interference constraint to restrict the resultant interference power under a predefined

value. Thus, the optimization problem can be formulated as

$$\begin{aligned} & \text{minimize}_{P_s(\omega, \gamma, h_{\text{sp}}) \geq 0} \mathcal{F}(\omega, P_s(\omega, \gamma, h_{\text{sp}})) \\ & \text{subject to } P_s(\omega, \gamma, h_{\text{sp}}) |h_{\text{sp}}|^2 \leq I_{\text{th}} \end{aligned} \quad (8)$$

where  $\gamma = \frac{|h_{\text{ss}}|^2}{1 + \bar{\gamma}_p |h_{\text{ps}}|^2}$  with  $\bar{\gamma}_p = P_p/N_0$ .

Since we consider the diverse preferences of different vehicular scenarios and interference constraints imposed by satellite communications, the transmit power of vehicular communications  $P_s$  is a function of  $\omega$ ,  $\gamma$ , and  $h_{\text{sp}}$ , i.e.,  $P_s(\omega, \gamma, h_{\text{sp}})$ .

In the following, we first provide a solution for the optimization problem without the interference constraint, i.e.,

$$\text{minimize}_{P_s(\omega, \gamma) \geq 0} \frac{(1 - \omega) \Psi_{\text{MAX}}^{\text{SE}} + \omega \Psi_{\text{MAX}}^{\text{EE}} \mathbb{E}_\gamma \{\eta P_s(\omega, \gamma) + P_0\}}{\mathbb{E}_\gamma \{\log_2(1 + P_s(\omega, \gamma) \gamma / N_0)\}}. \quad (9)$$

By denoting  $g(P_s(\omega, \gamma))$  and  $f(P_s(\omega, \gamma))$  as the numerator and denominator, respectively, (9) can be equalized to

$$\text{maximize}_{P_s(\omega, \gamma) \geq 0} \frac{f(P_s(\omega, \gamma))}{g(P_s(\omega, \gamma))}. \quad (10)$$

As observed, the objective function in (10) is a ratio of two functions with respect to  $P_s(\omega, \gamma)$ . According to Charnes-Cooper transformation [27], we apply suitable variable transformation to reformulate the optimization problem to an equivalent problem. By applying the transformation  $x = \frac{P_s}{G(P_s)}$  and  $t = \frac{1}{G(P_s)}$ , we have

$$\begin{aligned} & \text{maximize}_{P_s(\omega, \gamma) \geq 0} t f\left(\frac{x}{t}\right) \\ & \text{subject to } t g\left(\frac{x}{t}\right) \leq 1. \end{aligned} \quad (11)$$

*Theorem 2:* If  $(x^*, t^*)$  is an optimal solution for (11), then  $\frac{x^*}{t^*}$  is an optimal solution for (10).

*Proof:* The proof is presented in Appendix B. ■

Then, the optimization in (9) can be written as

$$\begin{aligned} & \text{maximize}_{P_s(\omega, \gamma) \geq 0} t \mathbb{E}_\gamma \{\log_2(1 + P_s(\omega, \gamma) \gamma / N_0)\} \\ & \text{subject to } t((1 - \omega) \Psi_{\text{MAX}}^{\text{SE}} + \omega \Psi_{\text{MAX}}^{\text{EE}} \mathbb{E}_\gamma \{\eta P_s(\omega, \gamma) + P_0\}) \leq 1. \end{aligned} \quad (12)$$

In the following, we focus on solving the optimization problem (12). As the objective function in (12) is a logarithmic function with respect to  $P_s(\omega, \gamma)$ , thus it is concave according to [35]. Besides, the constraint is an affine function and thus, the feasible set defined by constraint is a convex set. Therefore, the Karush-Kuhn-Tucker (KKT) conditions are both sufficient and necessary for the optimality of (12) [35]. We employ the Lagrange multiplier method to obtain the optimal solution of the transmit power. Then, the partial Lagrangian of problem (12) is given by

$$\begin{aligned} \mathcal{L}(P_s(\omega, \gamma), t, \ell) = & t \mathbb{E}_\gamma \{\log_2(1 + P_s(\omega, \gamma) \gamma / N_0)\} \\ & + \ell \left( 1 - t \left( (1 - \omega) \Psi_{\text{MAX}}^{\text{SE}} + \omega \Psi_{\text{MAX}}^{\text{EE}} \mathbb{E}_\gamma \right. \right. \\ & \left. \left. \times \{\eta P_s(\omega, \gamma) + P_0\} \right) \right) \end{aligned} \quad (13)$$

where  $\ell > 0$  is the Lagrangian parameter. Then, the KKT condition  $\frac{\partial \mathcal{L}(P_s(\omega, \gamma), t, \ell)}{\partial P_s(\omega, \gamma)} = 0$  can be written as

$$\frac{t\gamma}{\ln 2(P_s(\omega, \gamma)\gamma + N_0)} - t\ell\omega\eta\Psi_{\text{MAX}}^{\text{EE}} = 0. \quad (14)$$

Hence, the power allocation can be found as

$$\tilde{P}_s = \left[ \frac{1}{\alpha\omega} - \frac{N_0}{\gamma} \right]^+ \quad (15)$$

where  $\alpha = \ln 2\ell\eta\Psi_{\text{MAX}}^{\text{EE}}$  and  $[x]^+ = \max(0, x)$ . The optimal value of  $\ell$  can be found from the following equation

$$\mathbb{E}_\gamma \left\{ \log_2 \left( 1 + \tilde{P}_s\gamma/N_0 \right) \right\} - \ell \left( (1 - \omega)\Psi_{\text{MAX}}^{\text{SE}} + \omega\Psi_{\text{MAX}}^{\text{EE}} \left( \eta\mathbb{E}_\gamma \left\{ \tilde{P}_s \right\} + P_0 \right) \right) = 0. \quad (16)$$

Note that (16) only depends on  $\ell$  and is independent from  $t$ . The involved mean values can be derived as

$$\mathbb{E}[\tilde{P}_s] = Q_1 \frac{(\alpha\omega)^{-1}}{(\alpha\omega N_0)^{\tilde{\varepsilon}_{\text{ps}}}} G_{32}^{22} \times \left[ \frac{(1+K)\alpha\omega N_0}{b_{\text{ps}}^2} \middle| \begin{array}{l} 1 - \tilde{\varphi}_{\text{ps}}, 1 + \tilde{\varphi}_{\text{ps}}, 2 + \tilde{\varepsilon}_{\text{ps}} \\ \tilde{\varepsilon}_{\text{ps}}, 1 + p + \tilde{\varepsilon}_{\text{ps}} \end{array} \right] \quad (17)$$

and

$$\begin{aligned} & \mathbb{E} \left[ \log_2 \left( 1 + \frac{\tilde{P}_s\gamma}{N_0} \right) \right] \\ &= Q_1 \sum_{l=0}^L \frac{(-1)^l \Gamma(l+1)}{l(\alpha\omega N_0)^{\tilde{\varepsilon}_{\text{ps}}}} \\ & \times G_{32}^{22} \left[ \frac{(1+K)\alpha\omega N_0}{b_{\text{ps}}^2} \middle| \begin{array}{l} 1 - \tilde{\varphi}_{\text{ps}}, 1 + \tilde{\varphi}_{\text{ps}}, 1 + \tilde{\varepsilon}_{\text{ps}} \\ \tilde{\varepsilon}_{\text{ps}} - l, 1 + p + \tilde{\varepsilon}_{\text{ps}} \end{array} \right]. \quad (18) \end{aligned}$$

where  $\tilde{\varepsilon}_{\text{ps}} = \frac{\varphi_{\text{ps}} + \varepsilon_{\text{ps}}}{2}$  and  $\tilde{\varphi}_{\text{ps}} = \frac{\varphi_{\text{ps}} - \varepsilon_{\text{ps}}}{2}$ .

*Proof:* The derivation can be found in Appendix C. ■

Assume that we have obtained the transmit power allocated for the interference unconstrained optimization. When the interference constraint is considered, since  $h_{\text{sp}}$  remains unchanged for each specific transmission slot, the interference received at the satellite receiver is determined by the transmit power. In this situation, the interference constraint in (8) can be equalized to a transmit power constraint, i.e.,  $P_s(\omega, \gamma) \leq I_{\text{th}}/|h_{\text{sp}}|^2$ . Then, the solution for the problem (8) can be divided into two regions:

- 1)  $\tilde{P}_s \leq I_{\text{th}}/|h_{\text{sp}}|^2$ : In this case, the added interference constraint does not affect the optimal solution and hence, the optimal power of (8) is the same as that of (9), i.e.,  $P_s^* = \tilde{P}_s$ .
- 2)  $\tilde{P}_s > I_{\text{th}}/|h_{\text{sp}}|^2$ : If the transmit power for minimizing the unconstrained utility function is beyond the interference level allowed by satellite communications, it would be invalid for practical system application. In this case, to protect satellite communications, the optimal transmit power should be limited by the interference constraint, i.e.,  $P_s^* = I_{\text{th}}/|h_{\text{sp}}|^2$ .

In summary, the optimal transmit power of (8) can be expressed as

$$P_s^* = \min \left( \left[ \frac{1}{\alpha\omega} - \frac{N_0}{\gamma} \right]^+, \frac{I_{\text{th}}}{|h_{\text{sp}}|^2} \right). \quad (19)$$

By using the synthetic objective discussed in (7), the solution in (19) means the optimal transmit power that maximizes the system resource efficiency [39] under a given system configuration, i.e., a given  $w$ . In other words, the optimal solution of the transmit power provides a proper guideline for system operator to optimize the system resource.

#### IV. ANALYSIS OF THE OPTIMAL TRANSMIT POWER

In the previous section, we have investigated a power allocation strategy from the EE-SE tradeoff perspective and obtained the optimal transmit power solution expressed as a function of the preference factor. In this section, we conduct some discussions on the derived optimal transmit power. Firstly, the influence of the preference factor on the transmit power is analyzed. Moreover, utilizing the derived optimal transmit power, we theoretically analyze the performance of the cognitive satellite-vehicular networks in terms of OP, providing theoretical insights on the impacts of the preference parameter and interference constraints.

##### A. The Effect of $\omega$ on the Optimal Transmit Power

From (19) we can see that the optimal transmit power  $P_s^*$  is dependent on the interference constraint ( $I_{\text{th}}$ ), the channel gains ( $|h_{\text{ss}}|^2, |h_{\text{sp}}|^2, |h_{\text{ps}}|^2$ ), and the preference factor  $\omega$ , among which  $\omega$  is the decisive parameter in terms of the tradeoff between EE and SE. In the following, we focus on discussing the impact of  $\omega$  on  $P_s^*$ , where  $\omega$  can be divided into three regions:

- 1) when  $\omega < \frac{1}{\alpha} \left( \frac{N_0}{\gamma} + \frac{I_{\text{th}}}{|h_{\text{sp}}|^2} \right)^{-1}$ , the ratio of EE in utility function is too small to affect the transmit power allocation. In this case, the power allocation scheme can be regarded as an optimization problem maximizing SE. Thus, the transmit power equals to the maximum value bounded by interference constraints, i.e.,  $P_s^* = \frac{I_{\text{th}}}{|h_{\text{sp}}|^2}$ .
- 2) when  $\frac{1}{\alpha} \left( \frac{N_0}{\gamma} + \frac{I_{\text{th}}}{|h_{\text{sp}}|^2} \right)^{-1} \leq \omega \leq \frac{\gamma}{\alpha N_0}$ , we have  $P_s^* = \frac{1}{\alpha\omega} - \frac{N_0}{\gamma}$ . In this case, we should adjust the transmit power according to channel fading under the given preference factor  $\omega$ .
- 3) when  $\omega > \frac{\gamma}{\alpha N_0}$ , we have  $P_s^* = 0$ . Here, extremely poor link quality between vehicular users, such as serve fading, long distance, or serious interference from satellite, may result in vehicular communications being terminated. In this case, the reused resource for vehicular users can be reallocated to increase the spectrum access probability.

##### B. Outage Performance Based on the Optimal Transmit Power

To visualize the effect of the power allocation scheme on the transmission performance, we investigate the performance

of the secondary vehicular system in terms of OP based on the derived solution in (19). The OP,  $\mathcal{P}_{\text{out}}$ , is defined as the probability that the instantaneous end-to-end SINR falls below a threshold  $\Theta_{\text{th}}$ , i.e.,

$$\mathcal{P}_{\text{out}} = \Pr(\gamma_s \leq \Theta_{\text{th}}) \quad (20)$$

where  $\gamma_s = P_s^* \gamma / N_0$ . From (19), we can get

$$\gamma_s = \frac{P_s^* |h_{\text{ss}}|^2}{P_p |h_{\text{ps}}|^2 + N_0} = \min \left( \left[ \frac{\gamma}{\alpha \omega N_0} - 1 \right]^+, \frac{I_{\text{th}} \gamma}{|h_{\text{sp}}|^2 N_0} \right). \quad (21)$$

As for random variables  $a$  and  $b$ , we have  $\min(a, b) = a$  if  $b \geq a$  and  $\min(a, b) = b$  if  $b \leq a$ . Therefore,  $\mathcal{P}_{\text{out}}$  can be calculated as

$$\begin{aligned} \mathcal{P}_{\text{out}} = & \Pr \left( \frac{\gamma}{\alpha \omega N_0} - 1 \leq \frac{I_{\text{th}} \gamma}{|h_{\text{sp}}|^2 N_0}, \frac{\gamma}{\alpha \omega N_0} - 1 \geq 0, \frac{\gamma}{\alpha \omega N_0} - 1 \leq \Theta_{\text{th}} \right) \\ & + \Pr \left( \frac{\gamma}{\alpha \omega N_0} - 1 \geq \frac{I_{\text{th}} \gamma}{|h_{\text{sp}}|^2 N_0}, \frac{I_{\text{th}} \gamma}{|h_{\text{sp}}|^2 N_0} \leq \Theta_{\text{th}} \right). \end{aligned} \quad (22)$$

By carrying out some algebraic manipulations on (22),  $\mathcal{P}_{\text{out}}$  can be expressed as the sum of the following probabilities

$$\begin{aligned} \Xi_1 = & \Pr \left( \frac{\alpha \omega N_0 |h_{\text{sp}}|^2}{|h_{\text{sp}}|^2 - \alpha \omega I_{\text{th}}} \leq \gamma \leq \frac{\Theta_{\text{th}} N_0 |h_{\text{sp}}|^2}{I_{\text{th}}} \right) \\ = & \int_0^\infty \int_{\frac{\alpha \omega N_0 y}{y - \alpha \omega I_{\text{th}}}}^{\frac{\Theta_{\text{th}} N_0 y}{I_{\text{th}}}} f_\gamma(x) f_{|h_{\text{sp}}|^2}(y) dx dy \end{aligned} \quad (23)$$

$$\begin{aligned} \Xi_2 = & \Pr \left( |h_{\text{sp}}|^2 \geq \frac{\alpha \omega (\Theta_{\text{th}} + 1)}{\Theta_{\text{th}} I_{\text{th}}}, \alpha \omega N_0 \leq \gamma \leq \frac{\alpha \omega N_0 |h_{\text{sp}}|^2}{|h_{\text{sp}}|^2 - \alpha \omega I_{\text{th}}} \right) \\ = & \int_{\frac{\alpha \omega (\Theta_{\text{th}} + 1)}{\Theta_{\text{th}} I_{\text{th}}}}^\infty \int_{\alpha \omega N_0}^{\frac{\alpha \omega N_0 y}{y - \alpha \omega I_{\text{th}}}} f_\gamma(x) f_{|h_{\text{sp}}|^2}(y) dx dy \end{aligned} \quad (24)$$

$$\begin{aligned} \Xi_3 = & \Pr \left( |h_{\text{sp}}|^2 \leq \frac{\alpha \omega (\Theta_{\text{th}} + 1)}{\Theta_{\text{th}} I_{\text{th}}}, \alpha \omega N_0 \leq \gamma \leq \alpha \omega N_0 (\Theta_{\text{th}} + 1) \right) \\ = & \int_0^{\frac{\alpha \omega (\Theta_{\text{th}} + 1)}{\Theta_{\text{th}} I_{\text{th}}}} \int_{\alpha \omega N_0}^{\alpha \omega N_0 (\Theta_{\text{th}} + 1)} f_\gamma(x) f_{|h_{\text{sp}}|^2}(y) dx dy. \end{aligned} \quad (25)$$

According to the integral property, we firstly calculate the integrals of  $f_\gamma(x)$  with  $[0, \alpha \omega N_0]$ ,  $[0, \alpha \omega N_0 (\Theta_{\text{th}} + 1)]$ ,  $[0, \frac{\Theta_{\text{th}} N_0 y}{I_{\text{th}}}]$ , and  $[0, \frac{\alpha \omega N_0 y}{y - \alpha \omega I_{\text{th}}}]$ , which are denoted as  $\Delta_1$ ,  $\Delta_2$ ,  $\Delta_3$ , and  $\Delta_4$ , respectively. Then, we can get

$$\begin{aligned} \Delta_1 = & \int_0^{\alpha \omega N_0} f_\gamma(x) dx = Q_1 \int_0^{\alpha \omega N_0} x^{-\tilde{\epsilon}_{\text{ps}} - 1} \\ & \times G_{21}^{12} \left[ \frac{(1+K)}{b_{\text{ps}}^2} x \middle| \begin{matrix} 1 - \tilde{\varphi}_{\text{ps}}, 1 + \tilde{\varphi}_{\text{ps}} \\ 1 + p + \tilde{\epsilon}_{\text{ps}} \end{matrix} \right] dx. \end{aligned} \quad (26)$$

Using the integral relationship in [36, eq. (7.811.2)],  $\Delta_1$  can be computed as

$$\Delta_1 = \frac{Q_1}{(\alpha \omega N_0)^{\tilde{\epsilon}_{\text{ps}}}} G_{32}^{13} \left[ \frac{(1+K)\alpha \omega N_0}{b_{\text{ps}}^2} \middle| \begin{matrix} 1 + \tilde{\epsilon}_{\text{ps}}, 1 - \tilde{\varphi}_{\text{ps}}, 1 + \tilde{\varphi}_{\text{ps}} \\ 1 + p + \tilde{\epsilon}_{\text{ps}}, \tilde{\epsilon}_{\text{ps}} \end{matrix} \right]. \quad (27)$$

Similarly, we can obtain

$$\begin{aligned} \Delta_2 = & \frac{Q_1}{(\alpha \omega N_0 (\Theta_{\text{th}} + 1))^{\tilde{\epsilon}_{\text{ps}}}} \\ & \times G_{32}^{13} \left[ \frac{\alpha \omega N_0 (1+K) (\Theta_{\text{th}} + 1)}{b_{\text{ps}}^2} \middle| \begin{matrix} 1 + \tilde{\epsilon}_{\text{ps}}, 1 - \tilde{\varphi}_{\text{ps}}, 1 + \tilde{\varphi}_{\text{ps}} \\ 1 + p + \tilde{\epsilon}_{\text{ps}}, \tilde{\epsilon}_{\text{ps}} \end{matrix} \right] \end{aligned} \quad (28)$$

and

$$\begin{aligned} \Delta_3 = & \frac{I_{\text{th}}^{\tilde{\epsilon}_{\text{ps}}} Q_1}{(\Theta_{\text{th}} N_0 y)^{\tilde{\epsilon}_{\text{ps}}}} G_{32}^{13} \\ & \times \left[ \frac{(1+K)\Theta_{\text{th}} N_0}{b_{\text{ps}}^2 I_{\text{th}}} y \middle| \begin{matrix} 1 + \tilde{\epsilon}_{\text{ps}}, 1 - \tilde{\varphi}_{\text{ps}}, 1 + \tilde{\varphi}_{\text{ps}} \\ 1 + p + \tilde{\epsilon}_{\text{ps}}, \tilde{\epsilon}_{\text{ps}} \end{matrix} \right]. \end{aligned} \quad (29)$$

To make the derivation of  $\Delta_4$  tractable, we approximate the PDF of generalized- $K$  model using a Gamma distributed format with a shape parameter  $\vartheta$  and a scale parameter  $\eta$  [40], i.e.,

$$f_{\tilde{\gamma}_p | h_{\text{ps}}|^2}(x) = \frac{x^{\vartheta_{\text{ps}} - 1} e^{-\frac{x}{\eta_{\text{ps}} \tilde{\gamma}_p}}}{\Gamma(\vartheta_{\text{ps}}) (\eta_{\text{ps}} \tilde{\gamma}_p)^{\vartheta_{\text{ps}}}}, \quad x > 0 \quad (30)$$

where  $\vartheta_{\text{ps}} = \frac{\varphi_{\text{ps}} \epsilon_{\text{ps}}}{\varphi_{\text{ps}} + \epsilon_{\text{ps}} + 1}$  and  $\eta_{\text{ps}} = \Omega_{\text{ps}} / \vartheta_{\text{ps}}$ . In this way,  $f_\gamma(x)$  can be simplified as

$$f_\gamma(x) = Q_2 x^p \left( \frac{1}{\eta_{\text{ps}} \tilde{\gamma}_p} + (1+K)x \right)^{-\vartheta_{\text{ps}} - p - 1} \quad (31)$$

with  $Q_2 = \frac{e^{-K}}{\Gamma(\vartheta_{\text{ps}}) (\eta_{\text{ps}} \tilde{\gamma}_p)^{\vartheta_{\text{ps}}}} \sum_{p=0}^L \frac{K^p (1+K)^{p+1} \Gamma(\vartheta_{\text{ps}} + p + 1)}{(p!)^2}$ . Then, with the aid of [36, eq. (3.194.1)], we can get

$$\begin{aligned} \Delta_4 = & Q_2 \frac{(\eta_{\text{ps}} \tilde{\gamma}_p)^{\vartheta_{\text{ps}} + p + 1}}{p + 1} \left( \frac{\alpha \omega N_0 y}{y - \alpha \omega I_{\text{th}}} \right)^{p+1} \\ & \times {}_2F_1 \left( \vartheta_{\text{ps}} + p + 1, p + 1; p + 2; -\frac{(1+K)\eta_{\text{ps}} \tilde{\gamma}_p \alpha \omega N_0 y}{y - \alpha \omega I_{\text{th}}} \right) \end{aligned} \quad (32)$$

where  ${}_2F_1(a, b; c; z)$  is the Hypergeometric function and can be expressed as the sum of  $L$  series, i.e.,  ${}_2F_1(a, b; c; z) = \sum_{r=0}^L \frac{(a)_r (b)_r z^r}{(c)_r r!}$  [36, eq. (9.100)]. Here,  $(a)_r = \Gamma(a+r)/\Gamma(a)$  is the Pochhammer symbol. Thus,  $\Delta_4$  can be expressed as

$$\begin{aligned} \Delta_4 = & Q_2 \sum_{r=0}^L \frac{(\vartheta_{\text{ps}} + p + 1)_r (-1)^r (1+K)^r}{(p+r+1)r!} (\eta_{\text{ps}} \tilde{\gamma}_p)^{r + \vartheta_{\text{ps}} + p + 1} \\ & \times (\alpha \omega N_0)^{r + p + 1} \left( \frac{y}{y - \alpha \omega I_{\text{th}}} \right)^{r + p + 1} \end{aligned} \quad (33)$$

Then, from (23) we can get

$$\Xi_1 = \int_0^\infty (\Delta_3 - \Delta_4) f_{|h_{\text{sp}}|^2}(y) dy. \quad (34)$$

By substituting (29) and (33) into (34) and applying [36, eq. (7.813.1)], the analytical expression of  $\Xi_1$  can be obtained. In the similar way,  $\Xi_2$  and  $\Xi_3$  can also be derived. Detailed derivations are omitted here due to the limited space.

Finally, by summing up  $\Xi_1$ ,  $\Xi_2$ , and  $\Xi_3$ , a closed-form expression of  $\mathcal{P}_{\text{out}}$  can be obtained as shown in (35), as shown at the bottom of the next page, where  $\Upsilon(\cdot, \cdot)$  and  $\Gamma(\cdot, \cdot)$  are the lower and upper incomplete Gamma functions, respectively.

## V. RESULTS AND ANALYSIS

In this section, numerical results are provided to evaluate the proposed power allocation scheme and corroborate our theoretical analysis. In the simulations, we employ the path loss model  $PL = 128.1 + 37.6 \log_{10}(d[\text{in Km}])$  for terrestrial links and set  $\eta = 1.2$ ,  $\Theta_{\text{th}} = 1$  dB,  $N_0 = -114$  dBm, and

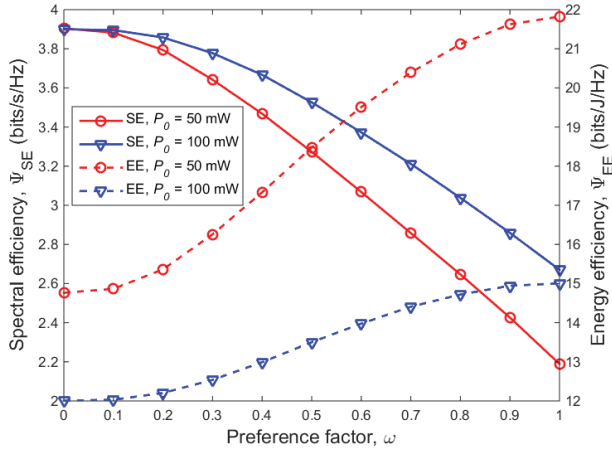


Fig. 3. EE and SE versus preference factor  $\omega$  for various  $P_0$  in a low VTD scenario with  $h_{sp}$  experiencing ILS fading ( $d_{ss} = 300$  m,  $v = 5$  m/s,  $\bar{\gamma}_p = 5$  dB,  $I_{th} = -95$  dBm).

$d_{sp} = 500$  m. For the generalized- $K$  fading channels, using a moment matching technique, the corresponding parameter  $\varphi_i$  can be linked to  $\varphi_i = \frac{1}{e^{\sigma^2} - 1}$ , where  $\sigma$  is the standard deviation of the log-normal shadowing and increases as the amount of fading increases. Considering the terrestrial link usually experiences a severer shadowing than the satellite downlink, we assume  $h_{ps}$  follows the infrequent light shadowing (ILS) fading, while  $h_{sp}$  follows the ILS fading or the average shadowing (AS) fading. Specifically, according to [41], we set  $\sigma_i = 0.115$ ,  $\varepsilon_i = 3$ ,  $\Omega_i = 1$  in ILS fading, while  $\sigma_i = 0.345$ ,  $\varepsilon_i = 2$ ,  $\Omega_i = 1$  in AS fading. Besides, the 3D V2V channel parameters are the same as configured in [26, Sec. IV].

We firstly conduct simulations to investigate the effects of the preference factor  $\omega$  on the corresponding EE and SE. Taking low VTD scenario as an example, Fig. 3 presents the SE (on the left-hand-side y-Axis) and EE (on the right-hand-side y-Axis) versus the preference factor  $\omega$  for various circuit power consumptions,  $P_0$ . It can be seen that the SE decreases while the EE gradually increases with increasing  $\omega$ . This phenomenon can be explained by the fact that increasing  $\omega$  raises the importance of EE and diminishes the priority of SE, which coincide with our design intention. Especially, in the case of  $\omega = 0$  and  $\omega = 1$ , the optimization reduces to the maximization of SE and EE, respectively. Additionally, different from EE, the expression of SE is independent of  $P_0$ . Thus, the SE curves with various  $P_0$  values overlap at the beginning while the EE curves have different endpoints. It is interesting to note that when  $\omega \in [0, 0.1]$ , EE and SE almost remain constant for  $P_0 = 50$  mW. This is because in

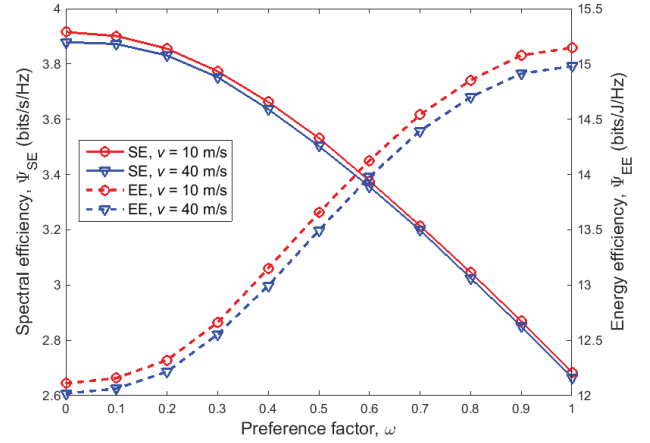


Fig. 4. EE and SE versus preference factor  $\omega$  for various velocities  $v$  in a low VTD scenario with  $h_{sp}$  experiencing ILS fading ( $d_{ss} = 300$  m,  $P_0 = 100$  mW,  $\bar{\gamma}_p = 5$  dB,  $I_{th} = -95$  dBm).

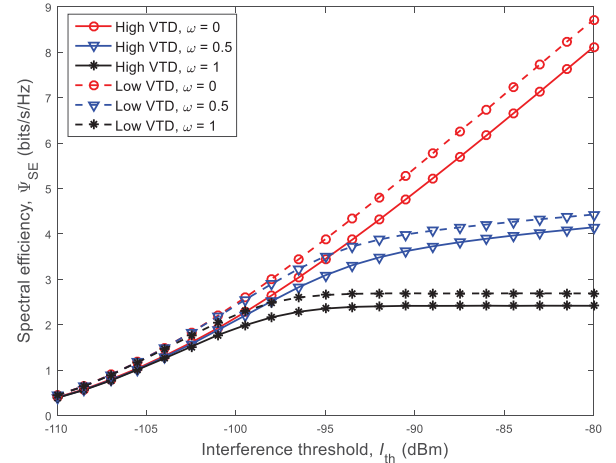


Fig. 5. SE versus interference threshold  $I_{th}$  for various preference factors  $\omega$  with  $h_{sp}$  experiencing ILS fading ( $d_{ss} = 300$  m,  $v = 5$  m/s,  $P_0 = 100$  mW,  $\bar{\gamma}_p = 5$  dB).

this region, the optimal transmit power is beyond the maximum allowable power bounded by interference constraints. Moreover, when  $P_0 = 100$  mW, we can achieve a higher SE while lower EE compared with  $P_0 = 50$  mW. This is because as  $P_0$  gets larger, the optimal transmit power would increase. To illustrate the impact of V2V channel characteristics on system performance, we plot the SE and EE versus the preference factor  $\omega$  for various vehicle velocities in Fig. 4. As observed, both the performance of SE and EE degrade as the velocity increases, which reveals that a larger velocity represents a poor communication link condition.

$$\begin{aligned}
 P_{out} = & \frac{Q_1}{\Gamma(\vartheta_{sp})} \left( \frac{I_{th}}{\Theta_{th} N_0 \eta_{sp}} \right)^{\tilde{\varepsilon}_{ps}} G_{42}^{14} \left[ \frac{(1+K)\Theta_{th} N_0 \eta_{sp}}{b_{ps}^2 I_{th}} \middle| 1 - \vartheta_{sp} + \tilde{\varepsilon}_{ps}, 1 + \tilde{\varepsilon}_{ps}, 1 - \tilde{\varphi}_{ps}, 1 + \tilde{\varphi}_{ps} \right] - \frac{Q_2 Q_3 (-\alpha \omega I_{th})^{\vartheta_{sp}}}{\Gamma(\vartheta_{sp}) \eta_{sp}^{\vartheta_{sp}} \Gamma(r+p+1)} \\
 & \times G_{12}^{21} \left[ -\frac{\alpha \omega I_{th}}{\eta_{sp}} \middle| -r-p-\vartheta_{sp}, -\vartheta_{sp}, 0 \right] + \frac{Q_2 Q_3}{\Gamma(\vartheta_{sp})} e^{-\frac{\alpha \omega I_{th}}{\eta_{sp}}} \sum_{q=0}^{r+p+\vartheta_{sp}} \binom{r+p+\vartheta_{sp}}{q} \Gamma[\vartheta_{sp}-q] \frac{1}{\eta_{sp}} \left( \frac{(\Theta_{th}+1)\alpha \omega}{\Theta_{th} I_{th}} - \alpha \omega I_{th} \right) \\
 & \times \left( \frac{\alpha \omega I_{th}}{\eta_{sp}} \right)^q - \frac{Q_1 \Delta_1}{\Gamma(\vartheta_{sp})} \Gamma\left(\vartheta_{sp}, \frac{(\Theta_{th}+1)\alpha \omega}{\Theta_{th} I_{th} \eta_{sp}}\right) + (\Delta_2 - \Delta_1) \frac{\gamma\left(\vartheta_{sp}, \frac{(\Theta_{th}+1)\alpha \omega}{\eta_{sp} \Theta_{th} I_{th}}\right)}{\Gamma(\vartheta_{sp})} \quad (35)
 \end{aligned}$$

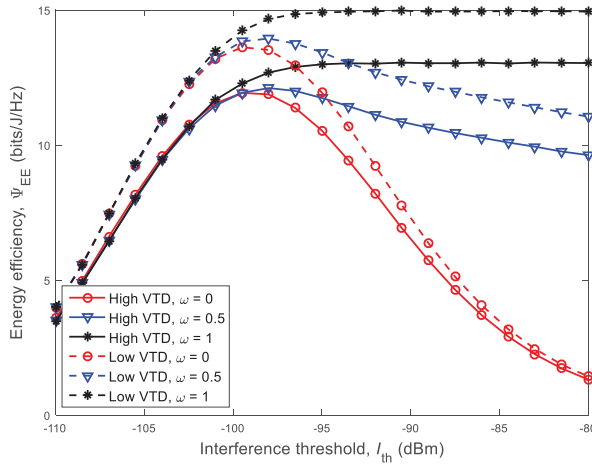


Fig. 6. EE versus interference threshold  $I_{th}$  for various preference factors  $\omega$  with  $h_{SP}$  experiencing ILS fading ( $d_{ss} = 300$  m,  $v = 5$  m/s,  $P_0 = 100$  mW,  $\bar{\gamma}_p = 5$  dB).

Then, we present the SE and EE versus the interference threshold  $I_{th}$  for various preference factors  $\omega$  in Fig. 5 and Fig. 6, respectively. For both figures, communication occurring in high VTD scenario experiences a worse performance than that in low VTD scenario, either in terms of SE or EE. This is due to the fact that in high VTD scenario, the received power is reflected by dense moving vehicles, which result in a smaller Ricean factor. Moreover, In the case of  $\omega = 0$  where the unified tradeoff optimization reduces to the SE maximization problem, the optimal transmit power is exactly the maximum allowable power bounded by interference power constraints. Thus, as the interference constraint gets looser, i.e.,  $I_{th}$  becomes larger, the optimal transmit power increases, resulting in a continuously growing in SE and simultaneously losing EE. When  $\omega = 1$ , the unified tradeoff optimization reduces to an EE maximization problem. In this case, from the figures we can observe that the maximum EE value can be achieved until  $I_{th}$  reaches to  $-95$  dBm which corresponds to the transmit power  $P_{EE}^*$ . Therefore, when  $I_{th} < -95$  dBm, SE and EE increase as  $I_{th}$  increases, while when  $I_{th} > -95$  dBm, system always operates at the global optimal power  $P_{EE}^*$ . As a result, EE stabilizes at its maximum value and SE remains at  $\Psi_{SE}(P_{EE}^*)$ .

Finally, we evaluate the outage performance based on the obtained optimal transmit power. Fig. 7 and Fig. 8 present the OP versus the satellite transmit power-to-noise ratio  $\bar{\gamma}_p$  and interference threshold  $I_{th}$ , respectively. For both figures, the outage performance in low VTD scenario outperforms that in high VTD scenario, which verifies our illustration in Section III. Moreover, we can observe that the theoretical results agree well with Monte Carlo simulations, confirming the accuracy of our derivations and simulations. For Fig. 7, as expected, the OP increases as  $\bar{\gamma}_p$  increases. Moreover, when the weight added on EE increases, i.e.,  $\omega$  gets larger, the optimal transmit power will decrease, which results in a poor outage performance. This phenomenon reveals that for a given system, there is a tradeoff between the reliability and energy efficiency. It is interesting to note that as  $\omega$  increase from 0.2 to 0.8 and finally to 1, the gaps between the corresponding curves get larger either in low VTD or high VTD scenarios,

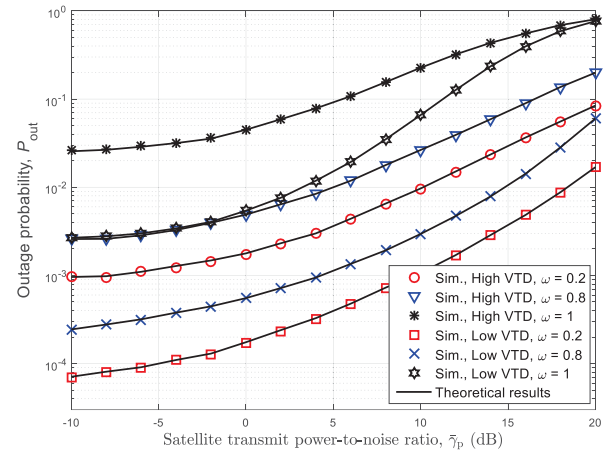


Fig. 7. OP versus satellite transmit power-to-noise ratio  $\bar{\gamma}_p$  for various  $\omega$  with  $h_{SP}$  experiencing ILS fading ( $d_{ss} = 300$  m,  $v = 10$  m/s,  $P_0 = 100$  mW,  $I_{th} = -80$  dBm).

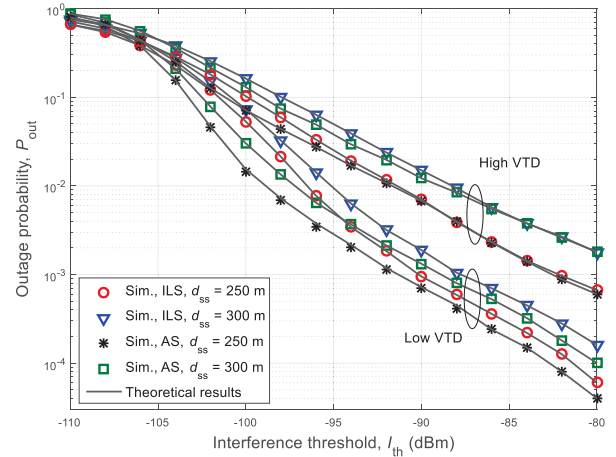


Fig. 8. OP versus interference threshold  $I_{th}$  for various  $d_{ss}$  and shadowing cases ( $v = 10$  m/s,  $\omega = 0.5$ ,  $\bar{\gamma}_p = -5$  dB,  $P_0 = 100$  mW).

which implies that the effect of the preference factor becomes more pronounced.

For Fig. 8, we can observe that the stricter the interference power constraint is, i.e.,  $I_{th}$  gets smaller, the larger the OP is, which verifies the fact that there is a balance between the performance of the primary and secondary systems. Moreover, when the vehicular transceivers are close to each other, i.e.,  $d_{ss}$  gets smaller, the channel condition will be improved and subsequently the outage performance. Furthermore, for a certain interference power constraint, when the interference link from the vehicular transmitter to the satellite receiver experiences severer fading, the optimal transmit power increases. Thus, the outage performance with AS shadowing outperforms that with ILS shadowing.

## VI. CONCLUSION

In this paper, we have proposed a power allocation scheme from the EE and SE tradeoff perspective in cognitive satellite-vehicular networks, where a 3D V2V channel model has been adopted. According to the distinct performance characteristics in different VTD scenarios, we have proposed a unified EE and SE tradeoff metric with a preference factor,

through which the priority level of EE and SE can be flexibly changed to adapt to various vehicular circumstances. By proving the utility function being strictly quasi-convex in transmit power, we have derived and analyzed a power allocation strategy under the interference power constraints imposed by satellite communications. Utilizing the obtained optimal transmit power, we have theoretically analyzed the outage performance of vehicular communications and discussed the impact of the preference factor on the optimal transmit power. Finally, numerical results have demonstrated that the developed EE-SE tradeoff metric can adapt to various vehicular circumstances and the interference power constraint is an effective method for co-channel interference management in cognitive systems.

#### APPENDIX A PROOF OF THEOREM 1

We rewrite  $\mathcal{F}(\omega, P_s)$  as

$$\mathcal{F}(\omega, P_s) = \frac{A + BP_s}{\log_2(1 + \nu P_s)} \quad (36)$$

where  $A = (1 - \omega)\Psi_{\text{MAX}}^{\text{SE}} + \omega P_0\Psi_{\text{MAX}}^{\text{EE}}$ ,  $B = \omega\eta\Psi_{\text{MAX}}^{\text{EE}}$ , and  $\nu = \frac{\gamma}{N_0}$ . From (36), we can get the first derivative of  $\mathcal{F}(\omega, P_s)$  as

$$\begin{aligned} \frac{\partial \mathcal{F}(\omega, P_s)}{\partial P_s} &= \frac{B \log_2(1 + \nu P_s) - \frac{\nu(A + BP_s)}{\ln 2(1 + \nu P_s)}}{(\log_2(1 + \nu P_s))^2} \\ &= \frac{h(P_s)}{(\log_2(1 + \nu P_s))^2} \end{aligned} \quad (37)$$

where  $h(P_s) = h_1(P_s) - h_2(P_s)$  with  $h_1(P_s) = B \log_2(1 + \nu P_s)$  and  $h_2(P_s) = \frac{\nu(A + BP_s)}{\ln 2(1 + \nu P_s)}$ .

For  $P_s \in [0, +\infty)$ , we have

$$\frac{\partial h(P_s)}{\partial P_s} = \frac{\nu^2(A + BP_s)}{\ln 2(1 + \nu P_s)^2}. \quad (38)$$

Since  $A > 0$ ,  $B > 0$ , and  $P_s > 0$ ,  $h'(P_s)$  is larger than zero for  $P_s \in [0, +\infty)$ . As  $h(P_s)$  is continuous, there is at most one intersection point between  $h_1(P_s)$  and  $h_2(P_s)$ . Moreover, let us assume that  $\tilde{P} \geq 0$ . If  $h_1(\tilde{P}) \geq h_2(\tilde{P})$ , we have  $h_1(P_s) > h_2(P_s)$  for  $P_s \geq \tilde{P}$ .

In addition, we have  $h(0) = h_1(0) - h_2(0) = -\frac{\nu A}{\ln 2} < 0$  and there is one intersection point  $\tilde{P}_s$  between  $h_1(P_s)$  and  $h_2(P_s)$ . For  $0 \leq P_s < \tilde{P}$ , we have  $h(P_s) < 0$ . Thus,  $\mathcal{F}(\omega, P_s)$  is strictly decreasing for  $0 \leq P_s < \tilde{P}$ . For  $P_s > \tilde{P}$ , we have  $h(P_s) > 0$ . Thus,  $\mathcal{F}(\omega, P_s)$  is strictly increasing for  $P_s > \tilde{P}$ . The minimum value of  $\mathcal{F}(\omega, P_s)$  can be obtained at  $P_s = \tilde{P}$ . Therefore,  $\mathcal{F}(\omega, P_s)$  is strictly quasi-convex in  $P_s \in [0, +\infty)$ . Hence, Theorem 1 follows.

#### APPENDIX B PROOF OF THEOREM 2

We denote  $F(x, t) = f\left(\frac{x}{t}\right)\varphi(t)$  and  $G(x, t) = g\left(\frac{x}{t}\right)\varphi(t)$ . For  $\vartheta > 0$ , we have  $G(x, t) = \vartheta$ . As  $(x^*, t^*)$  is an optimal solution of the optimization problem (11), we have

$$F(x^*, t^*) \geq F(x, t). \quad (39)$$

Let us assume that  $P_s = \frac{x^*}{t^*}$  is not the optimal solution of the problem (10). Thus, we have another value  $P_s^* \neq \frac{x^*}{t^*}$  that maximizes the objective function of (10), i.e.,

$$\frac{f(P_s^*)}{g(P_s^*)} > f\left(\frac{x^*}{t^*}\right) / g\left(\frac{x^*}{t^*}\right). \quad (40)$$

As the power consumption function is positive for all values of  $P_s$ , we have  $g(P_s^*) = \delta\vartheta$  ( $\delta > 0$ ). If we consider that  $x = P_s^*\varphi^{-1}(1/\delta)$  and  $t = \varphi^{-1}(1/\delta)$ , then  $(x, t)$  is a feasible solution for (11), i.e.,

$$G(x, t) = g(P_s^*)\varphi(t) = \vartheta. \quad (41)$$

Therefore, we can get the following expression

$$\frac{f(P_s^*)}{g(P_s^*)} = \frac{f(P_s^*)\varphi(t)}{g(P_s^*)\varphi(t)} = \frac{F(x, t)}{G(x, t)} = \frac{F(x, t)}{\vartheta}. \quad (42)$$

We also have

$$\frac{f(x^*/t^*)}{g(x^*/t^*)} = \frac{\varphi(t^*)f(x^*/t^*)}{\varphi(t^*)g(x^*/t^*)} = \frac{F(x^*, t^*)}{G(x^*, t^*)} = \frac{F(x^*, t^*)}{\vartheta}. \quad (43)$$

From (40), (42), and (43), we can conclude that

$$F(x^*, t^*) < F(x, t) \quad (44)$$

which contradicts the assumption that  $F(x^*, t^*) \geq F(x, t)$ . Thus,  $P_s = \frac{x^*}{t^*}$  is an optimal solution of (10). This completes the proof of Theorem 2.

#### APPENDIX C DERIVATION OF (17) AND (18)

From the expression of  $\tilde{P}_s$  specified in (15),  $\mathbb{E}_\gamma[\log_2(1 + \frac{\tilde{P}_s\gamma}{N_0})]$ , denoted by  $\bar{\Psi}_{\text{SE}}$ , can be calculated as

$$\begin{aligned} \bar{\Psi}_{\text{SE}} &= \mathbb{E}_\gamma \left[ \log_2 \left( \frac{v}{\alpha\omega N_0} \right) \right] \Big|_{\gamma \geq \alpha\omega N_0} \\ &= \int_{\alpha\omega N_0}^{\infty} \log_2 \left( \frac{x}{\alpha\omega N_0} \right) f_\gamma(x) dx. \end{aligned} \quad (45)$$

To calculate the integral in (45), we need to derive the PDF of  $\gamma$  firstly. From  $\gamma = \frac{|h_{\text{ss}}|^2}{1 + \tilde{\gamma}_p |h_{\text{pd}}|^2}$ ,  $f_\gamma(x)$  can be written as

$$f_\gamma(x) = \int_0^{\infty} (y + 1) f_{\tilde{\gamma}_p |h_{\text{ps}}|^2}(y) f_{|h_{\text{ss}}|^2}(x(y + 1)) dy. \quad (46)$$

By substituting (4) and (6) into (46) and expanding the series expression for  $I_0(x)$  [36, eq. (8.447.1)], (46) can be expressed as

$$\begin{aligned} f_\gamma(x) &= \frac{2b_{\text{ps}}^{\varphi_{\text{ps}} + \varepsilon_{\text{ps}}}(1 + K)e^{-K}}{\Gamma(\varphi_{\text{ps}})\Gamma(\varepsilon_{\text{ps}})(\tilde{\gamma}_p)^{\tilde{\varepsilon}_{\text{ps}}}} \sum_{p=0}^L \frac{K^p(1 + K)^p}{(p!)^2} x^p \\ &\quad \times \underbrace{\int_0^{\infty} y^{p + \tilde{\varepsilon}_{\text{ps}}} e^{-(1 + K)xy} K_{\varphi_{\text{ps}} - \varepsilon_{\text{ps}}}(2b_{\text{ps}}\sqrt{y}) dy}_J \end{aligned} \quad (47)$$

where  $\tilde{\varepsilon}_{\text{ps}} = \frac{\varphi_{\text{ps}} + \varepsilon_{\text{ps}}}{2}$ . In the above derivation, we assume that the interference dominates the noise, which is reasonable in an interference-limited scenario [37]. To derive the integral

in (47), we express  $K_{\varphi_{ps}-\varepsilon_{ps}}(2b_{ps}\sqrt{y})$  in terms of Meijer-j function [38, eq. (14)], i.e.,

$$K_{\varphi_{ps}-\varepsilon_{ps}}(2b_{ps}\sqrt{y}) = \frac{1}{2} G_{02}^{20} \left[ b_{ps}^2 y \middle| \begin{matrix} \cdot \\ \tilde{\varphi}_{ps}, -\tilde{\varphi}_{ps} \end{matrix} \right] \quad (48)$$

where  $\tilde{\varphi}_{ps} = \frac{\varphi_{ps}-\varepsilon_{ps}}{2}$ . Then, by substituting (48) into (47) and using [36, eq. (7.813.1)],  $J$  can be obtained as

$$J = \frac{1}{2} ((1+K)x)^{-p-\tilde{\varepsilon}_{ps}-1} G_{12}^{21} \left[ \frac{b_{ps}^2}{(1+K)x} \middle| \begin{matrix} -p-\tilde{\varepsilon}_{ps} \\ \tilde{\varphi}_{ps}, -\tilde{\varphi}_{ps} \end{matrix} \right]. \quad (49)$$

Utilizing the property of Meijer-j function shown in [36, eq. (9.31.2)],  $f_\gamma(x)$  can be given by

$$f_\gamma(x) = Q_1 x^{-\tilde{\varepsilon}_{ps}-1} G_{21}^{12} \left[ \frac{(1+K)}{b_{ps}^2} x \middle| \begin{matrix} 1-\tilde{\varphi}_{ps}, 1+\tilde{\varphi}_{ps} \\ 1+p+\tilde{\varepsilon}_{ps} \end{matrix} \right] \quad (50)$$

with  $Q_1 = \frac{b_{ps}^{\varphi_{ps}+\varepsilon_{ps}} e^{-K}}{\Gamma(\varphi_{ps})\Gamma(\varepsilon_{ps})(\tilde{\gamma}_p)^{\tilde{\varepsilon}_{ps}}} \sum_{p=0}^L \frac{K^p(1+K)^{-\tilde{\varepsilon}_{ps}}}{(p!)^2}$ .

Then, we focus on deriving  $\bar{\Psi}_{SE}$  in (45). Considering the fact that the integral in (45) is mathematically intractable, we expand the log function into the sum of  $L$  series and substitute  $f_\gamma(x)$  in (50) into (45). Then,  $\bar{\Psi}_{SE}$  can be calculated as

$$\begin{aligned} \bar{\Psi}_{SE} &= Q_1 \sum_{l=0}^L \frac{(-1)^l (\alpha\omega N_0)^{-l}}{l} \int_{\alpha\omega N_0}^{\infty} x^{-\tilde{\varepsilon}_{ps}-1} (x - \alpha\omega N_0)^l \\ &\quad \times G_{21}^{12} \left[ \frac{(1+K)}{b_{ps}^2} x \middle| \begin{matrix} 1-\tilde{\varphi}_{ps}, 1+\tilde{\varphi}_{ps} \\ 1+p+\tilde{\varepsilon}_{ps} \end{matrix} \right] dx. \end{aligned} \quad (51)$$

With the aid of [36, eq. (7.811.3)], the analytical expression of  $\bar{\Psi}_{SE}$  can be finally derived as shown in (18).

From the expression of  $\tilde{P}_s$  specified in (15), the average transmit power can be expressed as

$$\begin{aligned} \mathbb{E}_\gamma[\tilde{P}_s] &= \mathbb{E}_\gamma \left[ \frac{1}{\alpha\omega} - \frac{N_0}{x} \right] \bigg|_{\gamma \geq \alpha\omega N_0} \\ &= \int_{\alpha\omega N_0}^{\infty} \left( \frac{1}{\alpha\omega} - \frac{N_0}{x} \right) f_\gamma(x) dx. \end{aligned} \quad (52)$$

With the similar derivation steps of  $\bar{\Psi}_{SE}$ , the analytical expression of  $\mathbb{E}_\gamma[\tilde{P}_s]$  can be calculated as shown in (17).

## REFERENCES

- [1] M. Shaat, E. Lagunas, A. I. Perez-Neira, and S. Chatzinotas, "Integrated terrestrial-satellite wireless backhauling: Resource management and benefits for 5G," *IEEE Veh. Technol. Mag.*, vol. 13, no. 3, pp. 39–47, Sep. 2018.
- [2] X. Zhu *et al.*, "Cooperative multigroup multicast transmission in integrated terrestrial-satellite networks," *IEEE J. Sel. Areas Commun.*, vol. 36, no. 5, pp. 981–992, May 2018.
- [3] S. Kandeepan, L. De Nardis, M. G. Di Benedetto, A. Guidotti, and G. E. Corazza, "Cognitive satellite terrestrial radios," in *Proc. IEEE GLOBECOM*, Miami, FL, USA, Dec. 2010, pp. 1–6.
- [4] O. Y. Kolawole, S. Vuppala, M. Sellathurai, and T. Ratnarajah, "On the performance of cognitive satellite-terrestrial networks," *IEEE Trans. Cogn. Commun. Netw.*, vol. 3, no. 4, pp. 668–683, Dec. 2017.
- [5] M. Jia, X. Gu, Q. Guo, W. Xiang, and N. Zhang, "Broadband hybrid satellite-terrestrial communication systems based on cognitive radio toward 5G," *IEEE Wireless Commun.*, vol. 23, no. 6, pp. 96–106, Dec. 2016.
- [6] Y. Ruan, Y. Li, C.-X. Wang, R. Zhang, and H. Zhang, "Effective capacity analysis for underlay cognitive satellite-terrestrial networks," in *Proc. IEEE ICC*, Paris, France, May 2017, pp. 1–6.
- [7] "Electromagnetic compatibility and radio spectrum matters (ERM); system reference document; cognitive radio techniques for satellite communications operating in Ka band, v1.1.1," ETSI, Sophia Antipolis, France, Rep. TR 103 263, 2014.
- [8] H. Baek and J. Lim, "Spectrum sharing for coexistence of fixed satellite services and frequency hopping tactical data link," *IEEE J. Sel. Areas Commun.*, vol. 34, no. 10, pp. 2642–2649, Oct. 2016.
- [9] S. Maleki *et al.*, "Cognitive spectrum utilization in Ka band multi-beam satellite communications," *IEEE Commun. Mag.*, vol. 53, no. 3, pp. 24–29, Mar. 2015.
- [10] S. K. Sharma, S. Chatzinotas, and B. Ottersten, "Satellite cognitive communications: Interference modeling and techniques selection," in *Proc. IEEE ASMS/SPSC*, Baiona, Spain, Sep. 2012, pp. 111–118.
- [11] P. K. Sharma, P. K. Upadhyay, D. B. Costa, P. S. Bithas, and A. G. Kanas, "Performance analysis of overlay spectrum sharing in hybrid satellite-terrestrial systems with secondary network selection," *IEEE Trans. Wireless Commun.*, vol. 16, no. 10, pp. 6586–6601, Oct. 2017.
- [12] E. Lagunas, S. K. Sharma, S. Maleki, S. Chatzinotas, and B. Ottersten, "Resource allocation for cognitive satellite communications with incumbent terrestrial networks," *IEEE Trans. Cogn. Commun. Netw.*, vol. 1, no. 3, pp. 305–317, Sep. 2015.
- [13] S. Vassaki, M. I. Poulakis, A. D. Panagopoulos, and P. Constantinou, "Power allocation in cognitive satellite terrestrial networks with QoS constraints," *IEEE Commun. Lett.*, vol. 17, no. 7, pp. 1344–1347, Jul. 2013.
- [14] Z. Li, F. Xiao, S. Wang, T. Pei, and J. Li, "Achievable rate maximization for cognitive hybrid satellite-terrestrial networks with AF-relays," *IEEE J. Sel. Areas Commun.*, vol. 36, no. 2, pp. 304–313, Feb. 2018.
- [15] S. Shi, G. Li, K. An, Z. Li, and G. Zheng, "Optimal power control for real-time applications in cognitive satellite terrestrial networks," *IEEE Commun. Lett.*, vol. 21, no. 8, pp. 1815–1818, Aug. 2017.
- [16] J. Du *et al.*, "Secure satellite-terrestrial transmission over incumbent terrestrial networks via cooperative beamforming," *IEEE J. Sel. Areas Commun.*, vol. 36, no. 7, pp. 1367–1382, Jul. 2018.
- [17] B. Li *et al.*, "Robust chance-constrained secure transmission for cognitive satellite-terrestrial networks," *IEEE Trans. Veh. Technol.*, vol. 67, no. 5, pp. 4208–4219, May 2018.
- [18] T. M. Nguyen, A. T. Guillen, and S. S. Matsunaga, "Practical achievable capacity for advanced SATCOM on-the-move," in *Proc. IEEE MILCOM*, Baltimore, MD, USA, Nov. 2016, pp. 150–155.
- [19] G. Cocco, N. Alagha, and C. Ibars, "Cooperative coverage extension in vehicular land mobile satellite networks," *IEEE Trans. Veh. Technol.*, vol. 65, no. 8, pp. 5995–6009, Aug. 2016.
- [20] F. Alagoz and G. Gur, "Energy efficiency and satellite networking: A holistic overview," *Proc. IEEE*, vol. 99, no. 11, pp. 1954–1979, Nov. 2011.
- [21] Y. Ruan, Y. Li, C.-X. Wang, and R. Zhang, "Energy efficient adaptive transmissions in integrated satellite-terrestrial networks with SER constraints," *IEEE Trans. Wireless Commun.*, vol. 17, no. 1, pp. 210–222, Jan. 2018.
- [22] N. Yu, Z. Wang, H. Huang, and X. Jia, "Minimal energy broadcast for delay-bounded applications in satellite networks," *IEEE Trans. Green Commun. Netw.*, vol. 2, no. 3, pp. 795–803, Sep. 2018.
- [23] W. Zhang, C.-X. Wang, D. Chen, and H. Xiong, "Energy-spectral efficiency tradeoff in cognitive radio networks," *IEEE Trans. Veh. Technol.*, vol. 65, no. 4, pp. 2208–2218, Apr. 2016.
- [24] J. Zhang, B. Evans, M. A. Imran, X. Zhang, and W. Wang, "Green hybrid satellite terrestrial networks: Fundamental trade-off analysis," in *Proc. VTC-Spring*, Nanjing, China, May 2016, pp. 1–5.
- [25] R. Zhang *et al.*, "Energy-spectral efficiency trade-off in underlying mobile D2D communications: An economic efficiency perspective," *IEEE Trans. Wireless Commun.*, vol. 17, no. 7, pp. 4288–4301, Jul. 2018.
- [26] Y. Yuan, C.-X. Wang, X. Cheng, B. Ai, and D. I. Laurenson, "Novel 3D geometry-based stochastic models for non-isotropic MIMO vehicle-to-vehicle channels," *IEEE Trans. Wireless Commun.*, vol. 13, no. 1, pp. 298–309, Jan. 2014.
- [27] A. Charnes and W. W. Cooper, "Programming with linear fractional functionals," *Naval Res. Logistics Quart.*, vol. 9, no. 34, pp. 181–186, Sep./Oct. 1962.
- [28] L. T. Tan and L. B. Le, "Design and optimal configuration of full-duplex MAC protocol for cognitive radio networks considering self-interference," *IEEE Access*, vol. 3, pp. 2715–2729, 2015.

[29] K. P. Peppas, P. S. Bithas, G. P. Efthymoglou, and A. G. Kanatas, "Space shift keying transmission for intervehicular communications," *IEEE Trans. Intell. Transp. Syst.*, vol. 17, no. 12, pp. 3635–3640, Dec. 2016.

[30] S. Beygi, U. Mitra, and E. G. Ström, "Nested sparse approximation: Structured estimation of V2V channels using geometry based stochastic channel model," *IEEE Trans. Signal Process.*, vol. 63, no. 18, pp. 4940–4955, Sep. 2015.

[31] X. Ge, J. Chen, C.-X. Wang, J. S. Thompson, and J. Zhang, "5G green cellular networks considering power allocation schemes," *Sci. China Inf. Sci.*, vol. 59, no. 2, pp. 1–14, Feb. 2016.

[32] I. S. Ansari, S. Al-Ahmadi, F. Yilmaz, M.-S. Alouini, and H. Yanikomeroglu, "A new formula for the BER of binary modulations with dual-branch selection over generalized- $K$  composite fading channels," *IEEE Trans. Commun.*, vol. 59, no. 10, pp. 2654–2658, Oct. 2011.

[33] A. Paier *et al.*, "Non-WSSUS vehicular channel characterization in highway and urban scenarios at 5.2 GHz using the local scattering function," in *Proc. IEEE Int. ITG WSA*, Vienna, Austria, Feb. 2008, pp. 9–15.

[34] W. Sun, E. G. Ström, F. Brännström, K. C. Sou, and Y. Sui, "Radio resource management for D2D-based V2V communication," *IEEE Trans. Veh. Technol.*, vol. 65, no. 8, pp. 6636–6650, Aug. 2016.

[35] S. P. Boyd and L. Vandenberghe, *Convex Optimization*. Cambridge, U.K.: Cambridge Univ. Press, 2004.

[36] I. S. Gradshteyn and I. M. Ryzhik, *Table of Integrals, Series, and Products*, 6th ed. Boston, MA, USA: Academic, 2000.

[37] K. An *et al.*, "Performance analysis of multi-antenna hybrid satellite-terrestrial relay networks in the presence of interference," *IEEE Trans. Commun.*, vol. 63, no. 11, pp. 4390–4404, Nov. 2015.

[38] V. S. Adamchik and O. I. Marichev, "The algorithm for calculating integrals of hypergeometric type functions and its realization in reduce systems," in *Proc. Int. Conf. Symp. Algebraic Comput.*, Tokyo, Japan, 1990, pp. 212–224.

[39] J. Tang, D. So, E. Alsusa, and K. A. Hamdi, "Resource efficiency: A new paradigm on energy efficiency and spectral efficiency tradeoff," *IEEE Trans. Wireless Commun.*, vol. 13, no. 8, pp. 4656–4669, Aug. 2014.

[40] S. Al-Ahmadi and H. Yanikomeroglu, "On the approximation of the generalized- $K$  distribution by a gamma distribution for modeling composite fading channels," *IEEE Trans. Wireless Commun.*, vol. 9, no. 2, pp. 706–713, Feb. 2010.

[41] K. P. Peppas, "Accurate closed-form approximations to generalised- $K$  sum distributions and applications in the performance analysis of equal-gain combining receivers," *IET Commun.*, vol. 5, no. 7, pp. 982–989, May 2011.



**Yuhuan Ruan** received the B.S. and Ph.D. degrees in telecommunications engineering from Xidian University, Xi'an, China, in 2013 and 2018, respectively. She was a visiting Ph.D. student with Heriot-Watt University, Edinburgh, U.K., from 2016 to 2017, under the supervision of Prof. C.-X. Wang. She is currently a Post-Doctoral Fellow with Xidian University. Her research interests are in the fields of satellite-terrestrial networks, cooperative communications, cognitive radio techniques, and energy efficient wireless networks.



**Yongzhao Li** (M'04–SM'17) received the B.S., M.S., and Ph.D. degrees in electronic engineering from Xidian University, Xi'an, China, in 1996, 2001, and 2005, respectively. In 1996, he joined Xidian University, where he is currently a Full Professor with the State Key Laboratory of Integrated Services Networks and also currently serves as the Vice Dean of the Graduate School. He was a Research Professor with the University of Delaware, Delaware, USA, from 2007 to 2008, and the University of Bristol, Bristol, U.K., in 2011. He has published over 50 journal papers and 20 conference papers. His research interests include wideband wireless communications, signal processing for communications, and spatial communications networks. He was a recipient of the Best Paper Award of IEEE ChinaCOM'08 International Conference in 2008. Due to his excellent contributions in education and research, he was awarded by the Program for New Century Excellent Talents in University, Ministry of Education, China, in 2012.



**Cheng-Xiang Wang** (S'01–M'05–SM'08–F'17) received the B.Sc. and M.Eng. degrees in communication and information systems from Shandong University, China, in 1997 and 2000, respectively, and the Ph.D. degree in wireless communications from Aalborg University, Denmark, in 2004.

He was a Research Assistant with the Hamburg University of Technology, Hamburg, Germany, from 2000 to 2001, a Visiting Researcher with Siemens AG Mobile Phones, Munich, Germany, in 2004, and a Research Fellow with the University of Agder, Grimstad, Norway, from 2001 to 2005. He has been with Heriot-Watt University, Edinburgh, U.K., since 2005, where he was promoted to a Professor in 2011. In 2018, he joined Southeast University, China, as a Professor. He has authored 3 books, 1 book chapter, and over 350 papers in refereed journals and conference proceedings, including 23 Highly Cited Papers. He has also delivered 17 invited keynote speeches/talks and 6 tutorials in international conferences. His current research interests include wireless channel measurements and modeling, (B)5G wireless communication networks, and applying artificial intelligence to wireless communication networks.

Dr. Wang was a recipient of nine best paper awards from IEEE GLOBECOM 2010, IEEE ICCT 2011, ITST 2012, IEEE VTC 2013-Spring, IWCMC 2015, IWCMC 2016, IEEE/CIC ICC 2016, and WPMC 2016, and the Highly Cited Researcher Award by Clarivate Analytics in 2017 and 2018. He has served as the TPC member, the TPC chair, and the general chair for over 80 international conferences. He is currently an Executive Editorial Committee Member for the IEEE TRANSACTIONS ON WIRELESS COMMUNICATIONS. He has served as an Editor for nine international journals, including the IEEE TRANSACTIONS ON WIRELESS COMMUNICATIONS from 2007 to 2009, the IEEE TRANSACTIONS ON VEHICULAR TECHNOLOGY from 2011 to 2017, and the IEEE TRANSACTIONS ON COMMUNICATIONS from 2015 to 2017. He was a Guest Editor for the IEEE JOURNAL ON SELECTED AREAS IN COMMUNICATIONS, Special Issue on Vehicular Communications and Networks (Lead Guest Editor), Special Issue on Spectrum and Energy Efficient Design of Wireless Communication Networks, and Special Issue on Airborne Communication Networks. He was also a Guest Editor for the IEEE TRANSACTIONS ON BIG DATA, Special Issue on Wireless Big Data. He is a Fellow of IET and an IEEE Communications Society Distinguished Lecturer in 2019 and 2020.



**Rui Zhang** received the B.S., M.S., and Ph.D. degrees in telecommunications engineering from Xidian University, Xi'an, China, in 2012, 2015, and 2018, respectively. He was a visiting student with Heriot-Watt University, Edinburgh, U.K., from 2016 to 2017, under the supervision of Prof. C.-X. Wang. His current research interests focus on device-to-device communications, vehicle-to-vehicle communications, radio resource allocation techniques, and energy efficient wireless networks.



**Hailin Zhang** (M'98) received the B.S. and M.S. degrees from Northwestern Polytechnic University, Xi'an, China, in 1985 and 1988, respectively, and the Ph.D. degree from Xidian University, Xi'an, in 1991. Since 1991, he has been with Xidian University, where he is currently a Senior Professor and a Ph.D. Adviser with the School of Telecommunications Engineering. He is currently the Director of the Key Laboratory in Wireless Communications Sponsored by China Ministry of Information Technology, a Key Member of the State Key Laboratory of Integrated Services Networks, one of the State Government Specially Compensated Scientists and Engineers, a Field Leader in telecommunications and information systems with Xidian University, and the Associate Director for National 111 Project. He has recently published 78 papers in telecommunications journals and proceedings. His current research interests include key transmission technologies and standards on broadband wireless communications for 4G, 5G, and next generation broadband wireless access systems.